



Article

Sulfides in Metamorphic Rocks of the Fore Range Zone (Greater Caucasus). A New Type of Mineral Container for Peak Metamorphism Mineral Assemblages

Vladimir A. Kamzolkin ^{1,*}, Aleksandr N. Konilov ^{2,3}, Ekaterina P. Kulakova ¹,
Anton V. Latyshev ^{1,4}, Anna I. Smulskaya ¹ and Stanislav D. Ivanov ¹

¹ Schmidt Institute of the Physics of the Earth, Russian Academy of Sciences, 10 Bolshaya Gruzinskaya, 123242 Moscow, Russia; liverpool.town.uk@gmail.com (E.P.K.); anton.latyshev@gmail.com (A.V.L.); anna-smulskaya@mail.ru (A.I.S.); f0ma@ifz.ru (S.D.I.)

² Geological Institute, Russian Academy of Sciences, 7 Pyzhevskiy lane, 119017 Moscow, Russia; chalma@bk.ru

³ Institute of Experimental Mineralogy, Russian Academy of Sciences, 4 Academica Osypyana, Chernogolovka, 142432 Moscow, Russia

⁴ Geological Faculty, Lomonosov Moscow State University, 1 Leninsky Gory, 119992 Moscow, Russia

* Correspondence: vkamzolkin@gmail.com

Received: 26 September 2019; Accepted: 11 November 2019; Published: 13 November 2019



Abstract: The rocks of the Armovka Formation (the Fore Range zone, Greater Caucasus) have undergone low-grade metamorphism that partially erased information about initial rock formation conditions. We discovered high-pressure mineral inclusions such as omphacite, phengite, garnet, and paragonite enclosed by pyrite and chalcopyrite. Mineral inclusions in sulfides may provide important information about metamorphic pressure–temperature conditions because they are shielded by the host minerals and isolated from significant low-grade overprinting. Calculations performed on phengite inclusions using the phengite Si-content barometry indicate a pressure ranging from 1.7 ± 0.2 to 1.9 ± 0.2 GPa for temperature of 600 ± 40 °C. These data are consistent with estimations obtained for eclogite bodies embedded in rocks of the Armovka Formation. Geothermobarometry of the latest yielded conditions of 680 ± 40 °C and a minimum pressure of 1.6 ± 0.2 GPa to upper pressure boundary at 2.1 GPa. This fact allows us to assume that the metamorphic rocks of the Armovka Formation were immersed in the subduction zone to the conditions of the eclogite facies of metamorphism, forming a coherent subduction complex together with eclogites.

Keywords: mineral containers; pyrite; HP complexes; low-grade alteration

1. Introduction

A reliable determination of the thermodynamic parameters of metamorphic rocks processes, especially an estimation of their depth, is of high importance for identification of the Earth's crust structure. It is generally accepted that the temperature conditions of metamorphism depend on the proximity and power of the heat source and can change much faster in the crust than pressure, which is determined, first of all, by the lithostatic pressure [1]. Therefore, a sharp change in the P-parameters of metamorphic rocks is an evidence of tectonic disturbances such as large-scale nappes or thrust sheets in the crystalline crust. However, the task of determining pressure is far from simple, especially for complexes considered as of high pressure. Overprinting by retrograde processes can almost completely change the mineral assemblage of rocks, making difficult to recognize earlier metamorphic conditions or removing all information about peak conditions. Minerals stable in a wide range of

pressure–temperature (P – T) conditions are able to be containers and preserve phases characteristic of sedimentary, magmatic, or metamorphic processes as inclusions. For example, ultra-high-pressure conditions can be identified by the occurrence of coesite or diamond preserved in high-density mechanically strong host minerals such as garnet or zircon, which are less susceptible to destruction during overprinting processes [2].

It is known that the eclogites are the main indicators of high-pressure during metamorphism [3]. They consist mainly of garnet with a high content of pyrope and Na clinopyroxene (omphacite), with minor amounts of quartz, rutile, and some other minerals. It is usually assumed that eclogites formed during rapid sinking (subduction) of cold oceanic lithosphere to the depths corresponding to at least the upper mantle [4,5]. In geological sections, eclogites and often associated with them garnet–glaucophane schists, are found not among the rocks of ancient oceanic crusts (ophiolites), but among rocks of the continental crust, including those that formed in its upper part [6]. Coexistence of rock types from various geneses at the surface can result from eventual exhumation as a tectonic mélange within subduction channels [7–10]. However, in many cases metasedimentary rocks and orthogneisses, which are host for eclogite bodies, are strongly modified by late stage low-grade metamorphism, leading to partially or completely overprinting primary mineral assemblages and making it difficult to recognize earlier metamorphic conditions. The important question during every research of orogenic belts is whether such rocks should generally be considered as part of high-pressure complexes, i.e., petrologically coherent with the eclogites. The structurally consistent occurrence of eclogites among acid ortho- or paragneisses does not definitely solve this question, since apparent structural conformity can appear as a result of large general superimposed deformation under different pressure parameters. Therefore, petrological data attesting high pressure of the host gneisses are of particular importance.

In most host rocks of eclogites from the Fore Range zone of the Greater Caucasus, rock matrix is strongly altered by low-grade overprinting and does not contain indicator minerals of high-pressure conditions. However, these minerals were positively found as inclusions in sulfide mineral containers, namely pyrite and chalcopyrite. Such finding reveals the potential of sulfides as a new type of container minerals, and also confirms the high-pressure nature of the eclogites host rocks. A preliminary survey suggests that some of the micro-inclusions in garnets within the same eclogite-bearing gneisses and mica schists might also reflect high-pressure metamorphic conditions, although this is out of the scope of the present study, which is focused on the minerals in the sulfides.

2. Geological Setting

Theoretical hypotheses on geological structure of the Greater Caucasus change quite quickly as new petrological, geophysical, and geochronological data become available. Main review papers on geology, tectonics, and geodynamics of the Caucasus belong to Gamkrelidze and Shengelia [11], Adamia et al. [12], and Somin [6]. The Fore Range zone is the oldest and the most strongly metamorphosed zone (up to high-pressure (HP) conditions of metamorphism compared with low pressure (LP) type of metamorphism of another tectonic units of the Greater Caucasus [6]). The Fore Range zone has a general nappe structure. The rocks of the crystalline basement are overlain by a pack of thrust sheets of Paleozoic (Silurian–Early Carboniferous) age and different genesis: Urup and Kizilkol–Tokhana volcanic–sedimentary, Marukh ophiolitic, and Atsgara metamorphic complexes [6]. The thrust sheets are overlain in turn by Lower–Middle Carboniferous–Permian molasses in the upper part (Figure 1). The crystalline basement of the Fore Range zone is exposed in several salients of various size, including the largest Blyb salient, where rocks of the Blyb metamorphic complex occur. Until recently, it was believed that the Blyb metamorphic complex was represented by the Balkan mafic Formation cut by the Balkan quartz metadiorite massif and the Armovka Formation [6]. The U–Pb data from rocks of the Balkan massif yielded Ediacaran ages (549–574 Ma) [13] while garnet–mica schists and paragneisses of the Armovka Formation provided an age of 362.2 ± 1.9 and 361.4 ± 3.0 Ma, respectively [14,15]. Hence, according to structural, isotopic, petrographic, and rock-magnetic studies, the tectonic coupling

of the Balkan Formation and spatially associated rocks of the Armovka Formation appears evident and the Armovka Formation is interpreted as a nappe independent from the Balkan tectonic unit [13]. In turn, the Armovka Formation is tectonically overlain by greenschist facies metavolcanic rocks of the Late Silurian–Middle Devonian Urup complex.

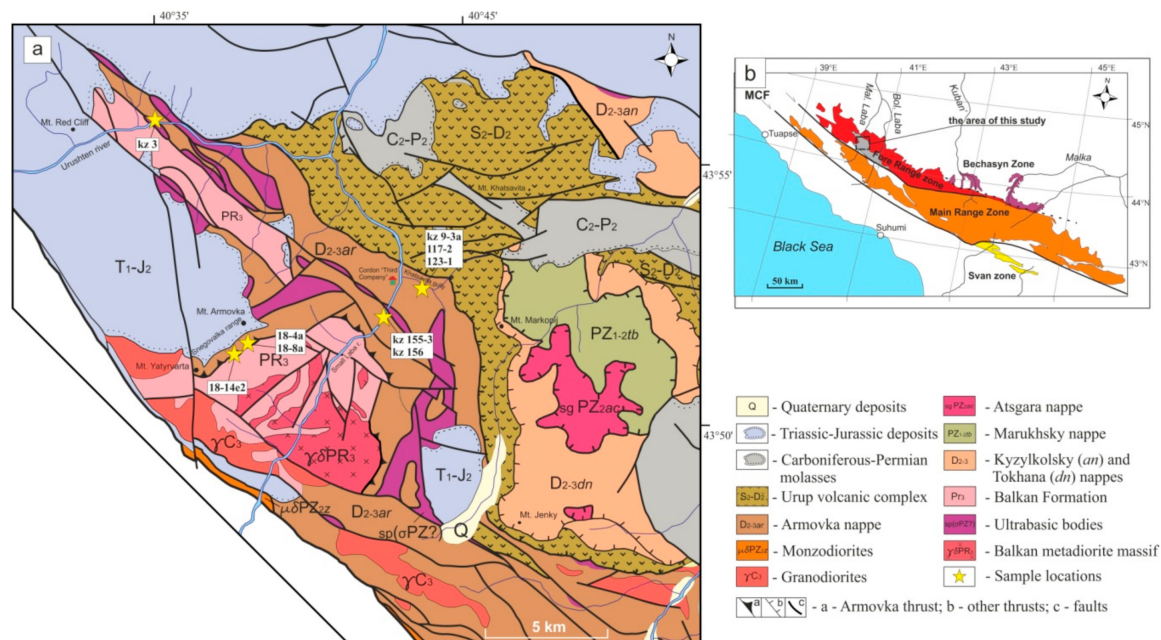


Figure 1. (a) Local geological scheme of the Blyb salient area (compiled on base of map 1:200,000 of [16] with changes); (b) tectonic scheme of the pre-Mesozoic basement of the Greater Caucasus. MCF—Main Caucasus Fault.

The Armovka Formation consists of interlayered gneisses, epidote-bearing amphibolites, and garnet–mica schists, with minor massive and banded mafic eclogites and ultramafic rocks. It should be noted that eclogite facies rocks within the Blyb salient occur exclusively in the Armovka Formation [17]. The first reports on eclogites findings date back to the 70s of the 20th century and belong to Afanas'ev G., Ploshko V., Shport N., Tatrishvili N., Knyazeva D. (unfortunately, all publications only in Russian) [18–21], and later these and some other eclogite bodies were studied by Somin M., Korikovski S., Perchuk A., Gerasimov V., and other authors [6,22]. Within the Armovka Formation, eclogites occur as sheet-like bodies up to 100 m in length and up to 15 m in thickness embedded in garnet–mica schists, orthogneisses or amphibolites [21,23], and sometimes associated with serpentinite bodies. Estimations of P – T conditions of metamorphism for eclogites and host rocks are scarce [22,24]. It should be noted, that the structural evolution of the Blyb salient area has been poorly studied so far.

3. Materials and Methods

3.1. Methods

The Armovka Formation rocks were studied at different distant outcrops bordering the Blyb salient. Polished thin sections were prepared from all samples and then observed under a Nikon Eclipse LV100 Pol optical microscope at the Institute of Experimental Mineralogy of Russian Academy of Sciences (IEM RAS) in Chernogolovka, Moscow region or an Olympus BX53M optical microscope at the Schmidt Institute of the Physics of the Earth of Russian Academy of Sciences (IPE RAS) in Moscow. Nine samples of particular interest due to their content of sulfides with inclusions were selected for additional scanning electron microscopy study. Locations of studied samples are shown in Figure 1 and given in Table 1.

Table 1. GPS coordinates and mineral assemblages of studied samples.

Sample	Lithology	Coordinates	Mineral Assemblage
kz 9-3a	Epidote gneiss	N 43.88461° E 40.73036°	Pl + Ms + Ep + Qtz + Py + Chl + Rt
117-2	Epidote gneiss	N 43.88433° E 40.73408°	Pl + Ep + Ms + Chl + Py +Qtz
123-1	Epidote gneiss	N 43.88861° E 40.74458°	Pl + Ms + Ep + Py + Chl + Cal
kz 155-3	Epidote–amphibole gneiss	N 43.87614° E 40.70458°	Pl + Amp + Ep + Ms + Chl + Bt + Py + Rt + Qtz + Cal
kz 3	Garnet–epidote–amphibole gneiss	N 43.94592° E 40.59233°	Pl + Ms + Amp + Grt + Ep + Qtz + Py + Chl + Rt
18-8a	Garnet–epidote–amphibole gneiss	N 43.86403° E 40.63769°	Pl + Ms + Qtz + Amp + Grt + Chl + Py + Rt + Ep
18-14e2	Epidote amphibolite	N 43.85811° E 40.63567°	Pl + Amp + Ep + Bt + Ms + Chl + Py + Qtz
18-4a	Garnet–epidote amphibolite	N 43.86308° E 40.64050°	Amp + Qtz + Ep + Grt + Ms + Chl + Mag + Rt + Py
kz 156	Garnet–muscovite blastomylonite	N 43.87231° E 40.70889°	Grt + Ms + Pl + Ep + Amp + Chl + Py + Ccp + Rt

Note: Amp—amphibole; Bt—biotite; Cal—calcite; Ccp—chalcopyrite; Chl—chlorite; Ep—epidote; Grt—garnet; Mag—magnetite; Ms—muscovite; Pl—plagioclase; Py—pyrite; Qtz—quartz; Rt—rutile. Mineral abbreviations are after Whitney and Evans [25].

The chemical compositions of the minerals, whose grain size is on the order of 2–5 µm, or larger, were determined using a Tescan Vega II XMU scanning electron microscope with an INCA Energy 450 energy dispersive spectrometer (EDS), equipped with an INCA x-sight semiconductor Si(Li) detector (Oxford Instruments) at the IEM RAS. The operating conditions were: 20 kV accelerating voltage, beam current ~350 pA on element (Co) for quant optimization, and a beam diameter of 1–5 µm. Acquisition time was 70 s. The chemical composition was calculated with the INCA ver. 4.15 software from the Microanalysis Suite Issue 18 + SP3 software package. Secondary electron (SE) and backscattered electron (BSE) images were obtained also using the Tescan Vega II XMU scanning electron microscope at the IEM RAS.

Raman analysis was carried out using a Senterra Raman spectrometer (by Bruker) at the IEM RAS.

3.2. Petrography

Metamorphic rocks of the Armovka Formation are presented by both metapelites and metabasites. According to our observations, metapelites are presumably garnet-mica schists, sometimes containing kyanite. Garnet forms porphyroblastic grains up to 5 mm in size, often with secondary chlorite in cracks. The mineral assemblage is garnet + muscovite (paragonite) ± kyanite + chlorite + quartz + rutile and magnetite. Ca-rich rocks of the Armovka Formation, or metabasites, are mainly epidote–garnet amphibolites. Amphibolites contain amphibole, garnet, epidote, white mica, biotite, plagioclase, chlorite, quartz, and Fe–Ti oxides and sulfides (rutile, magnetite, pyrite, chalcopyrite). Modal amounts of minerals differ from layer to layer including rocks with dominant garnet content (> 50 modal %) described as garnetites. Metabasites often contain secondary “cribriform” plagioclase containing inclusions of matrix minerals such as amphibole, epidote, and muscovite, while primary plagioclase is almost absent. Typical accessory minerals are rutile, titanite, apatite, pyrite, and chalcopyrite with the proportion of sulfides reaching up to 5% of the rock volume.

Studied nine sulfide-bearing rocks were porphyroblastic epidote (kz 9-3a, 117-2, 123-1), epidote–amphibole (kz 155-3) and garnet–epidote–amphibole (kz 3, 18-8a) gneisses, epidote (18-14e2) and garnet–epidote (18-4a) amphibolites, and garnet–muscovite blastomylonite (kz 156) from the Armovka Formation (Figure 2).

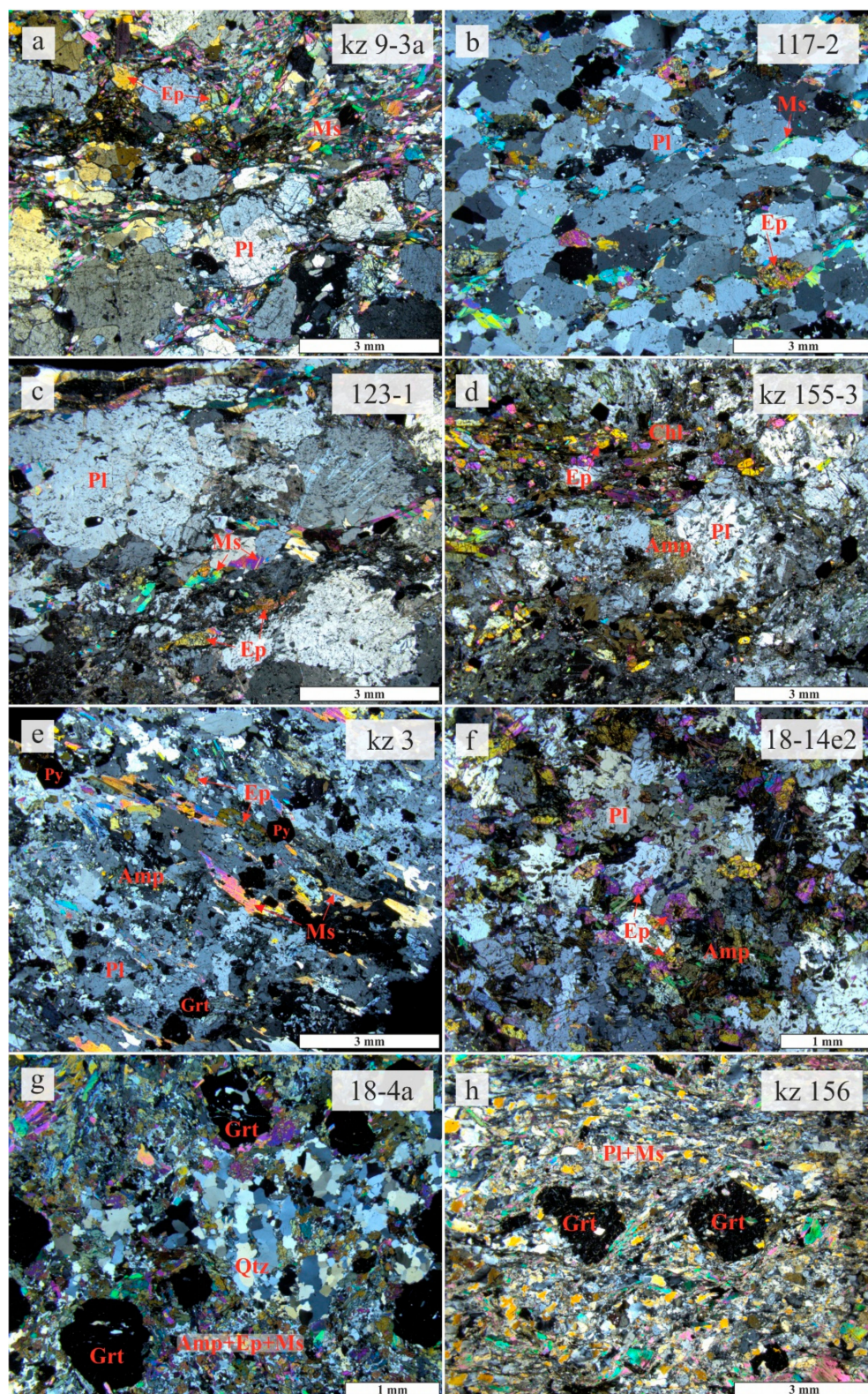


Figure 2. Thin sections of studied Armovka Formation rocks in transmitted, cross-polarized light. Mineral abbreviations are after [25]: Amp—amphibole; Chl—chlorite; Ep—epidote; Grt—garnet; Ms—muscovite; Pl—plagioclase; Py—pyrite; Qtz—quartz. (a–c) Epidote gneisses with plagioclase porphyroblasts, (d) epidote–amphibole gneiss with plagioclase porphyroblasts, (e) garnet–epidote–amphibole gneiss, (f) epidote amphibolite, (g) garnet–epidote amphibolite with garnet porphyroblasts and superimposed quartz vein, (h) garnet–muscovite blastomylonite with garnet porphyroblasts and foliation due to orientation of plagioclase and muscovite.

All gneisses contain plagioclase (40–50 vol%), muscovite, phengite, epidote, chlorite, sulfides, rutile, with variable amounts of amphibole, quartz (presumably of superimposed origin), garnet, biotite, magnetite and zircon. Epidote and epidote–amphibole gneisses contain coarse poikiloblastic porphyroblasts of plagioclase (albite) (Figure 2a,c,d). There are epidote, muscovite, and amphibole inclusions in porphyroblasts of plagioclase. There is a prevailing grain orientation in the thin sections mainly due to muscovite and epidote (Figure 2a–e).

Amphibolites have massive structure and porphyroblastic texture due to plagioclase (18-14e2) and garnet grains (18-4a). Sample 18-14e2 is an epidote amphibolite with primary amphibole + epidote + plagioclase (magmatic fragments) assemblage. Late albitization is associated with appearance of coarse-grained (up to 3 mm) plagioclase porphyroblasts, which contain inclusions of matrix minerals (Figure 2f). Sample 18-4a contains porphyroblastic garnet (ca. 2 mm), main matrix minerals are amphibole (40 vol%), epidote (10 vol%), muscovite (7 vol%), rutile, and sulfides (2 vol%). The sample has abundant amount of superimposed quartz veins (Figure 2g).

Garnet–muscovite blastomylonite (kz 156) is composed of garnet, muscovite, plagioclase, amphibole, epidote, chlorite, rutile, and pyrite. Sample has porphyroblastic structure due to garnet grains (up to 2 mm). Garnets contain inclusions of muscovite, plagioclase, quartz, and rutile; they are cracked and replaced by chlorite. Plagioclase and muscovite are main matrix minerals, and their orientation defines a foliation of the rock (Figure 2h).

The main matrix minerals in all samples demonstrate signs of alteration under low-temperature conditions. There is abundant matrix chlorite, which replaces biotite, muscovite, and garnet. Plagioclases in samples 123-1 and kz 156 are saussuritized, and secondary carbonates occur in kz 155-3 and 123-1 thin sections. Samples 123-1, 117-2, 18-4a, and 18-8a depict cross-cutting quartz lenses and veins.

4. Results and Discussion

4.1. Sulfides

Sulfides in the Armovka Formation rocks are mainly pyrite (Py, FeS₂) and rare chalcopyrite (Ccp, CuFeS₂). Chalcopyrite occurs both as grains in the matrix and as inclusions in pyrite. Sulfides are rather irregular xenoblastic, rarely subhedral. They have a rounded or elongated shape, but sometimes preserve straight grain edges and sharp ends (Figure 3). The grain sizes vary from tens up to 300 μm. Sulfides show evidence of late deformation resulting in cracking of grains and orientation of clusters of fragments along the foliation.

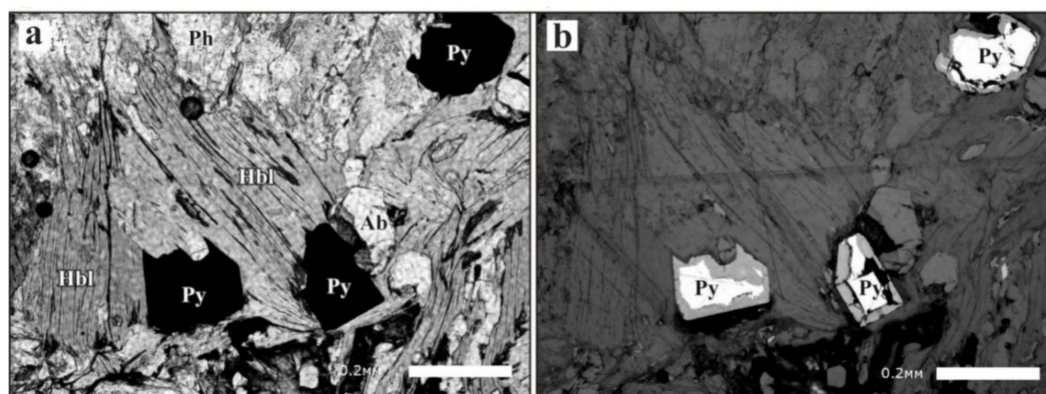


Figure 3. Thin section of pyrite-bearing amphibole–mica schist. Ab—albite; Hbl—hornblende; Py—pyrite; Ph—phengite. Photomicrographs are obtained in transmitted plane polarized (a) and reflected (b) light. Mineral abbreviations are after [25].

Sulfides of the studied rocks contain phengite, paragonite, garnet, epidote, amphibole, zircon, rutile, and quartz inclusions and also a mineral indicator of eclogite facies conditions—omphacite $Jd_{41}Ae_{18}$ (Figures 4 and 5). The presence of omphacite is also confirmed by Raman spectroscopy. Inclusions are commonly xenoblastic and rounded, and have size up to 40–50 μm . The data on the composition of inclusions in sulfides obtained for eleven samples are given in Tables 2 and 3. Moreover, inclusions of sulfates (anhydrite and barite) are also found in pyrite. Typically, these minerals are of sedimentary origin and are likely relic phases indicating a partially sedimentary origin for the protolith of the studied rocks.

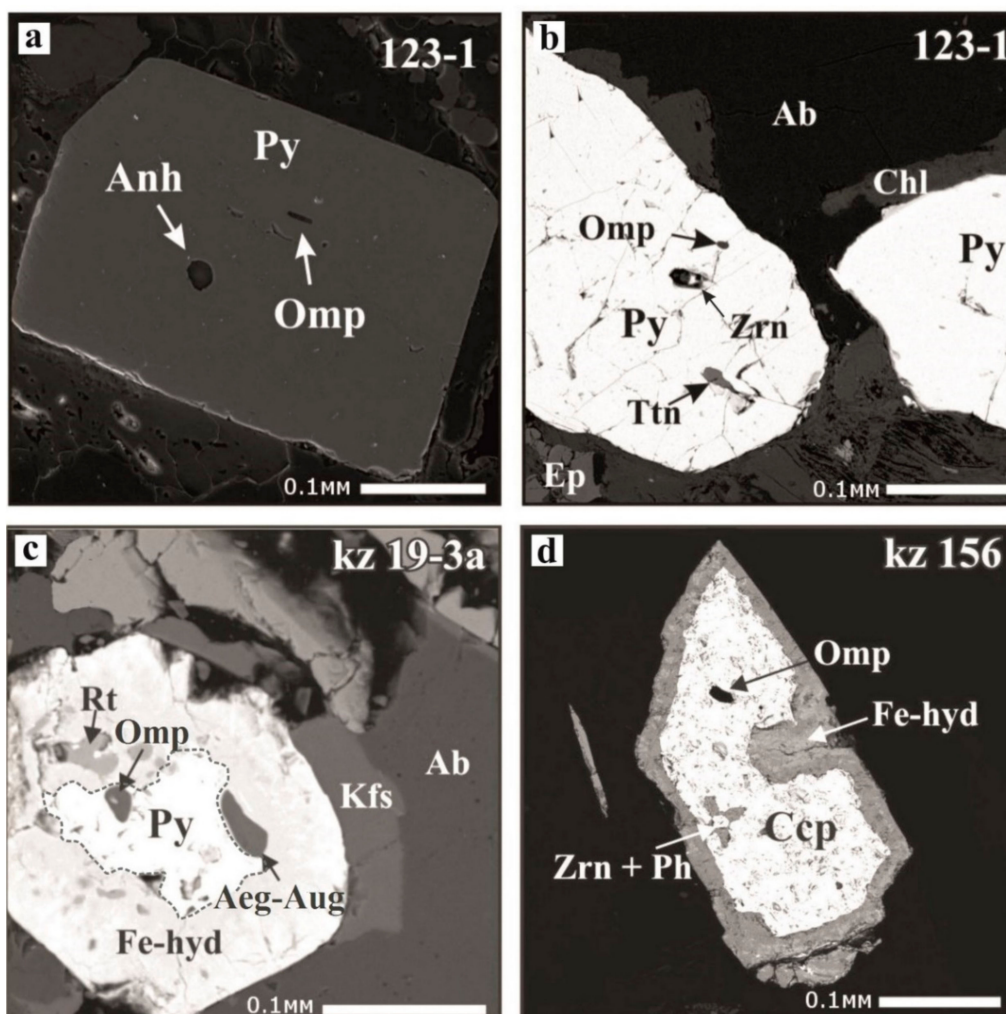


Figure 4. Photomicrographs of pyrites and chalcopyrite of the Armovka Formation containing various mineral inclusions. (a) Secondary electron (SE) image. (b–d) Backscattered electron (BSE) images. Grey rims surrounding sulfides are replacements of pyrite and chalcopyrite by Fe hydroxides (Fe-hyd). The sample number is in the upper right corner. Ab—albite; Aeg–Aug—aegirine-augite; Anh—anhydrite; Ccp—chalcopyrite; Chl—chlorite; Fe-hyd—Fe hydroxides; Kfs—K-feldspar; Omp—omphacite; Ph—phengite; Py—pyrite; Rt—rutile; Ttn—titanite; Zrn—zircon.

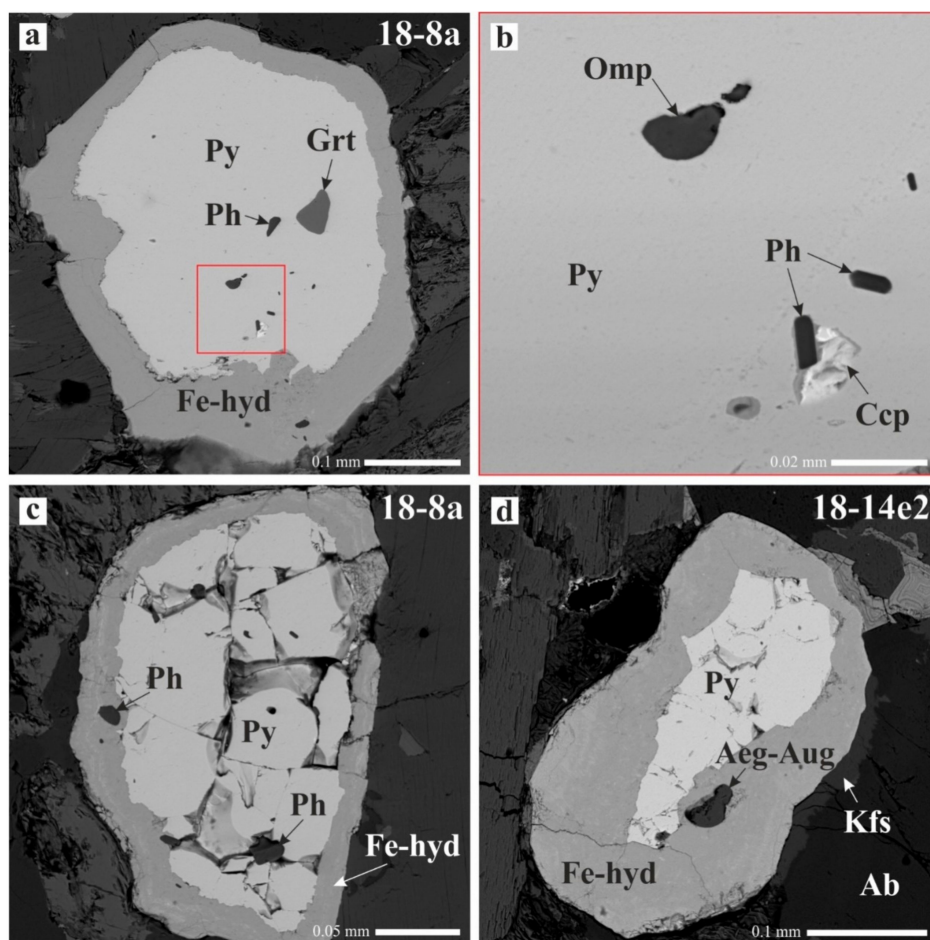


Figure 5. Photomicrographs of pyrites of the Armovka Formation containing various mineral inclusions. Backscattered electron images (BSE). Grey rims surrounding sulfides are replacements of pyrite by Fe hydroxides (Fe-hyd). (a) Garnet and phengite inclusions in pyrite. (b) Enlarged image of red rectangle area in Figure 5a; inclusions of omphacite, phengite, and chalcopyrite in pyrite grain. (c) Phengite inclusions in pyrite and in Fe-hyd rim surrounding pyrite. (d) Aegirine-augite inclusion located in zone of replacement of pyrite by Fe-hyd. Ab—albite; Aeg—aeirine; Aug—augite; Ccp—chalcopyrite; Fe-hyd—Fe hydroxides; Grt—garnet; Kfs—K-feldspar; Omp—omphacite; Ph—phengite; Py—pyrite.

Table 2. Representative phengite and paragonite electron microprobe analyses (wt. %).

Sample	117-2			Kz3	18-8a		
Inclusion	Ph 10	Ph 1	Pg 1	Ph 11	Ph 7	Ph 8	Ph 12
Host-Mineral	Py	Fe-hyd	Py	Py	Py	Fe-hyd	Fe-hyd
SiO ₂	46.88	46.55	45.28	48.09	45.99	46.33	46.6
TiO ₂	0.56	0.72	0.26	0.24	0.83	0.18	0.54
Al ₂ O ₃	29.31	28.05	39.47	26.84	26.96	26.39	25.59
Cr ₂ O ₃	0.00	0.53	0.27	0.06	0.10	0.02	0.00
FeO	5.44	4.71	1.72	3.16	3.16	4.50	4.28
MnO	0.00	0.37	0.34	0.10	0.00	0.00	0.27
MgO	3.53	1.57	0.05	2.78	2.64	2.53	3.05
CaO	0.20	0.08	0.38	0.00	0.02	0.00	0.18
Na ₂ O	0.77	1.16	6.65	0.82	1.20	1.00	1.08
K ₂ O	9.81	9.98	0.78	9.41	8.67	9.40	9.57
BaO	0.87	0.52	0.00	0.68	1.21	0.78	0.28
Total	97.37	94.24	95.20	92.18	90.78	91.13	91.44

Table 2. Cont.

Sample	117-2			Kz3		18-8a	
Si	3.148	3.185	2.926	3.348	3.269	3.260	3.264
Al ^{IV}	0.852	0.815	1.074	0.652	0.731	0.740	0.736
Al ^{VI}	1.468	1.447	1.932	1.550	1.527	1.449	1.376
Ti	0.028	0.038	0.013	0.013	0.044	0.010	0.029
Cr	0.000	0.029	0.014	0.003	0.006	0.001	0.000
Fe ³⁺	–	0.270	–	–	–	0.265	0.260
Fe ²⁺	0.306	0.000	0.093	0.184	0.188	0.000	0.000
Mn	0.000	0.022	0.019	0.006	0.000	0.000	0.016
Mg	0.353	0.160	0.005	0.289	0.280	0.266	0.318
Ca	0.014	0.006	0.026	0.000	0.002	0.000	0.014
Na	0.100	0.154	0.833	0.111	0.165	0.136	0.146
K	0.840	0.871	0.064	0.836	0.786	0.844	0.855
Ba	0.023	0.014	0.000	0.019	0.034	0.022	0.008
Total	7.134	7.010	7.000	7.010	7.031	6.993	7.022
O	11	11	11	11	11	11	11
X _{Mg}	0.536	–	0.026	0.611	0.598	–	–

Note: Fe-hyd—the zone of retrograde overprinting of sulfides; Ph—phengite; Pg—paragonite; Py - pyrite. X_{Mg} = Mg/(Mg + Fe²⁺).

The occurrence of metamorphic minerals as inclusions in pyrites was also reported by Li et al. [26], who found garnet, omphacite, glaucophane, phengite, epidote, and rutile in large pyrite grains of sulfide-bearing eclogites, blueschists, and high-pressure veins crosscutting eclogites. Most of those rocks preserved these minerals in their matrix and only a few of them were subjected to strong retrograde changes, which led to the almost complete absence of matrix omphacite (only as inclusions in garnet or pyrite or in the core domain of overprinted amphibole) and the appearance of abundant matrix albite, chlorite, and amphibole. Overall, the evolution of sulfide-bearing high-pressure rocks of the Akeyazi terrane (NW China) [26] and retrograde overprints (fracturing and recrystallization, chloritization, albitization) is broadly comparable to our Caucasian rocks but illustrates a stage before the significant low-grade metamorphism that affected the Armovka Formation.

Sulfides are commonly rimmed and replaced by Fe hydroxides pseudomorphs (Figure 4c,d and Figure 5a,c,d) of variable composition (Table 4). Results of representative major compositions assign these Fe hydroxides to a group of ferrihydrite (SiO₂ content of 2–4 wt. %) or limonite (SiO₂ content <1 wt. %). Raman spectroscopy of these pseudomorphs has given complex spectra of difficult interpretation, including spectra of Fe hydroxides and oxides such as goethite (Fe³⁺O(OH)), hematite (Fe₂O₃), erdite (NaFeS₂·2H₂O), etc. These data most likely indicate the heterogeneous structure of the substance. BSE images (see Figures 4d and 5a,c,d) of altered areas of sulfide grains confirm the conclusion about the heterogeneous structure, similar to a solid colloidal solution.

Pseudomorphic rims also contain mineral inclusions of amphibole, white mica, albite, and Na clinopyroxene of aegirine-augite composition (Na₂O = 8.8–10, Al₂O₃ = 10.3–12.7 wt. %). All studied clinopyroxene inclusions were plotted on the Jd–Ae–Q diagram of Morimoto et al. [27] (Figure 6). All inclusions in pyrite or chalcopyrite are presented by omphacite, whereas aegirine-augite is found only in altered rims of sulfides. We assume that hypergenic changes lead to oxidation of Fe²⁺ to Fe³⁺, so, aegirine-augite is the result of omphacite alteration (Figure 4c).

Garnet in inclusions is essentially almandine with significant contents of grossular, less so of pyrope, and minor amounts of andradite. Its composition can be expressed by the formula—Alm_{0.61} Grs_{0.20} Prp_{0.16} Adr_{0.03}. White mica inclusions are phengite and paragonite. Si-contents of phengite are 3.15–3.35 p.f.u. (per formula unit), which attests its formation at high-pressure conditions [28]. The conditions for paragonite formation cover a wide range, however, the coexistence of phengite and paragonite in the same sample (for example, sample 18-8a) also indicates high pressures [29].

Table 3. Representative garnet, epidote, amphibole, and clinopyroxene electron microprobe analyses (wt. %).

Sample	18-8a	18-4a	Kz 155-3	117-2	18-8a	18-14e2	Kz 156	123-1	Kz 9-3a	117-2				
Inclusion	Gr _t 10	Ep 6	Amp 19	Amp 11	Omp 14	Omp 6	Omp 1	Omp 3	Omp 8	Omp 13	Omp 14	Aeg-Aug 3	Aeg-Aug 20	Aeg-Aug 22
Host-Mineral	Py	Fe-hyd	Py	Fe-hyd	Py	Fe-hyd	Ccp	Py	Py	Py	Py	Fe-hyd	Fe-hyd	Fe-hyd
SiO ₂	38.02	36.32	50.37	43.57	54.32	52.16	55.00	53.68	57.13	54.24	52.32	53.78	50.32	49.86
TiO ₂	0.35	0.13	0.45	0.36	0.24	0.26	0.19	0.35	0.00	0.09	0.32	0.23	1.29	0.59
Al ₂ O ₃	21.28	27.27	11.74	9.29	11.20	7.54	12.58	8.58	10.86	10.44	9.46	9.96	12.09	12.31
Cr ₂ O ₃	0.26	0.07	0.00	0.43	0.00	0.06	0.00	0.00	0.07	0.04	0.00	0.17	0.00	0.00
FeO *	29.21	5.71	12.33	23.26	7.76	7.88	7.07	12.83	10.64	9.18	9.50	9.82	13.87	16.58
MnO	0.02	0.05	0.00	0.27	0.19	0.10	0.00	0.12	0.33	0.18	0.30	0.00	0.00	0.48
MgO	4.26	0.17	11.79	7.93	5.90	8.38	5.46	4.60	5.66	5.47	5.74	6.86	5.38	4.94
CaO	8.56	22.74	4.91	9.73	10.06	15.07	9.34	7.33	8.65	9.97	9.93	10.65	7.51	6.19
Na ₂ O	0.08	0.07	5.67	2.09	7.90	4.98	9.00	8.84	9.76	8.42	7.68	8.48	9.54	9.02
K ₂ O	0.04	0.00	0.39	0.23	0.13	0.00	0.00	0.00	0.05	0.01	0.06	0.05	0.00	0.01
Total	102.08	92.53	97.65	97.16	97.70	96.43	98.64	96.33	103.15	98.04	95.31	100.00	100.00	100.00
Si	2.951	2.967	7.191	6.738	1.986	1.963	1.973	2.012	1.972	1.979	1.973	1.918	1.802	1.803
Al ^{IV}	0.049	0.033	0.809	1.262	0.014	0.037	0.027	0.000	0.028	0.021	0.027	0.082	0.198	0.197
Al ^{VI}	1.947	2.592	1.169	0.432	0.469	0.298	0.505	0.379	0.414	0.428	0.393	0.336	0.312	0.328
Ti	0.020	0.008	0.050	0.042	0.007	0.007	0.005	0.010	0.000	0.002	0.009	0.006	0.035	0.016
Cr	0.016	0.005	0.000	0.053	0.000	0.002	0.000	0.000	0.002	0.001	0.000	0.005	0.000	0.000
Fe ³⁺	0.066	0.390	0.000	0.000	0.098	0.085	0.137	0.220	0.267	0.184	0.180	0.293	0.415	0.470
Fe ²⁺	1.833	0.000	1.472	3.008	0.139	0.163	0.075	0.182	0.040	0.096	0.120	0.000	0.000	0.032
Mn	0.001	0.003	0.000	0.035	0.006	0.003	0.000	0.004	0.010	0.006	0.010	0.000	0.000	0.015
Mg	0.493	0.021	2.511	1.828	0.322	0.470	0.292	0.257	0.291	0.297	0.323	0.365	0.287	0.266
Ca	0.712	1.990	0.751	1.612	0.394	0.608	0.359	0.294	0.320	0.390	0.401	0.407	0.288	0.240
Na	0.012	0.011	1.572	0.627	0.560	0.363	0.626	0.642	0.653	0.596	0.562	0.586	0.662	0.633
K	0.004	0.000	0.073	0.045	0.006	0.000	0.000	0.000	0.002	0.000	0.003	0.002	0.000	0.000
Total	8.039	8.020	15.590	15.683	4	4	4	4	4	4	4	4	4	4
O	12	12.5	23	23	6	6	6	6	6	6	6	5.988	5.968	6.000
X _{Mg}	0.21	–	0.63	0.38	–	–	–	–	–	–	–	–	–	–
JD, %					48.6	29.1	50.0	43.4	40.8	42.3	40.0	31.5	29.9	29.8
AE, %					10.1	8.3	13.6	25.2	26.3	18.2	18.3	27.5	39.8	42.7
WEF, %					41.3	62.6	36.4	31.4	32.9	39.5	41.7	41.0	30.3	27.5

Note: FeO * = total Fe as FeO. JD: Jadeite; AE: Aegirine; WEF: Wollastonite + enstatite + ferrosilite; Fe³⁺ was calculated assuming stoichiometric mineral; Aeg-Aug—aegirine-augite; Amp—amphibole; Ccp—chalcopyrite; Ep—epidote; Fe-hyd—the zone of retrograde overprinting of sulfides; Gr_t—garnet; Omp—omphacite; Py—pyrite. $X_{Mg} = Mg/(Mg + Fe^{2+})$; JD = $100 \cdot Na \cdot Al^{VI} / (Ca + Na)(Fe^{3+} + Al^{VI})$; AE = $100 \cdot Na \cdot Fe^{3+} / (Ca + Na)(Fe^{3+} + Al^{VI})$; WEF = 100-JD-AE.

Table 4. Representative major compositions of pyrite rims (wt. %).

Sample	117-2		18-8a	18-14e2
Analysis	2	21	13	3
SiO ₂	2.96	3.16	2.04	1.02
TiO ₂	0.03	0.03	0.16	0.00
Al ₂ O ₃	0.00	0.25	0.13	0.14
Cr ₂ O ₃	0.00	0.00	0.07	0.00
FeO *	77.74	76.61	73.37	72.68
MnO	0.00	0.00	0.01	0.00
MgO	0.93	3.08	0.38	0.00
CaO	0.25	0.03	0.00	0.20
Na ₂ O	0.00	0.00	0.16	0.10
K ₂ O	0.00	0.06	0.00	0.10
Total	81.91	83.22	76.60	74.52

Note: FeO * = total Fe as FeO.

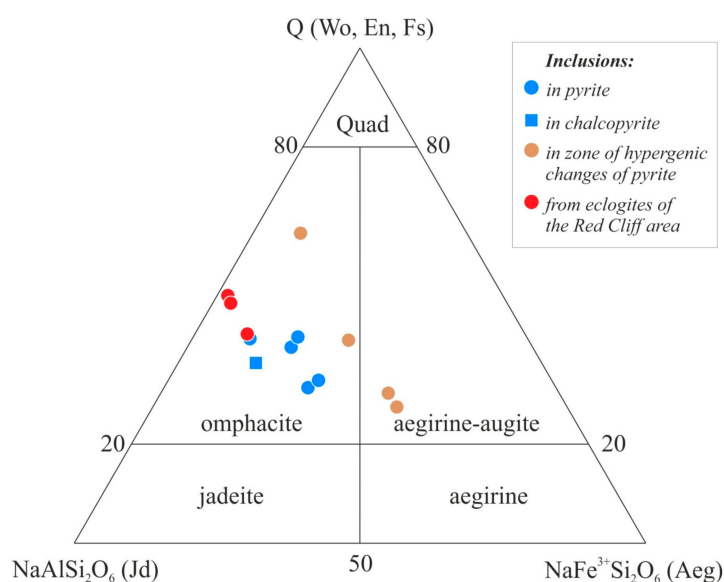


Figure 6. Compositions of analyzed clinopyroxene inclusions on the Jd–Ae–Q diagram of [27]. For comparisons, clinopyroxenes from eclogites of the Red Cliff area, Greater Caucasus [1] are also plotted (red points). Quad represents the Ca–Mg–Fe pyroxene area. Wo—wollastonite; En—enstatite; Fs—ferrosilite; Jd—jadeite; Aeg—aegirine.

4.2. P–T Estimates

Representative electron-microprobe analyses of phengite inclusions can be used to evaluate the pressure for a given temperature. According to published data, the temperature of metamorphism of the schists of the Armovka Formation is estimated at 600 ± 40 °C using the garnet–biotite Fe–Mg exchange thermometer [23]. We performed calculations using the phengite Si-content barometer of [30] (Figure 7). The pressure was calculated for temperatures from 560 to 640°. Data for all phengite inclusions at each temperature were averaged and the confidence interval was calculated using the Student’s t-test. The obtained pressure estimates are presented in Table 5. Accepting a temperature estimation of 600 ± 40 °C as the conditions of phengite formation, the calculations performed using phengite Si-content barometer indicate a pressure ranging from 1.7 ± 0.2 to 1.9 ± 0.2 GPa.

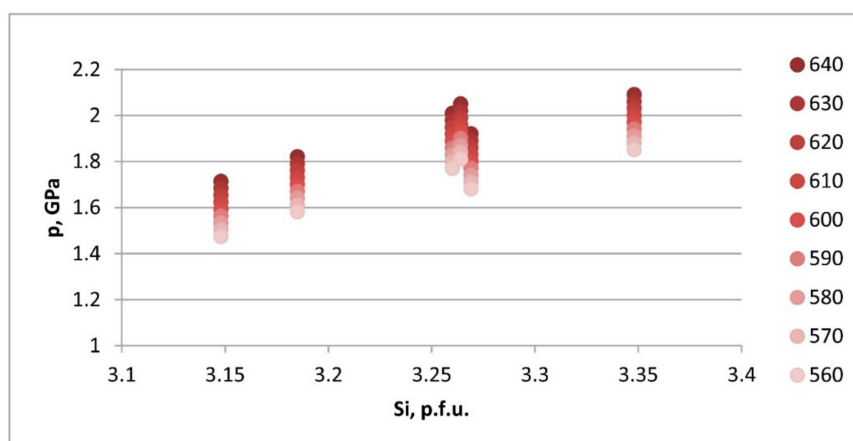


Figure 7. Pressure versus Si-content (per formula unit) calculated for every ten degrees for temperature range of 600 ± 40 °C using phengite barometer of [30].

Table 5. Mean calculated values of pressure for temperature of 600 ± 40 °C using the phengite Si-content barometry of [30].

Temperature	Pressure, GPa
560	1.69
570	1.72
580	1.75
590	1.78
600	1.81
610	1.84
620	1.87
630	1.90
640	1.93
Confidence interval	± 0.15

The omphacite inclusions in pyrite and chalcopyrite are similar in composition to omphacite from eclogite bodies exposed in the Red Cliff area of the Greater Caucasus (Figure 6), the geothermobarometry of which yielded conditions of 680 ± 40 °C and minimum pressure of 1.6 ± 0.2 GPa [23]. The upper pressure boundary for a temperature of 680 °C and water activity $a_{\text{H}_2\text{O}} = 1$ is evaluated at 2.1 GPa. These data on omphacite compositions are in good agreement with the results obtained from phengite barometry.

Hereby, the estimations of *P–T* conditions for mineral inclusions in sulfides of the Armovka Formation gneisses, mica schists, and amphibolites clearly attest to a high-pressure metamorphism that may be correlated to the metamorphic conditions of embedded eclogites. This allows us to argue that metapelitic and metabasic rocks of the Armovka Formation are structurally coherent to eclogites and they are likely to have been immersed together during subduction process.

4.3. Low-Grade Metamorphism

Most rocks of the Armovka Formation underwent low-grade metamorphism and rarely retain relict mineral assemblages of previous metamorphic stages. Here, we present photomicrographs of typical changes in the rocks of the Armovka Formation during their evolution, not only in studied sulfide-bearing samples. The degree of retrograde alteration varies for the different types of rocks but the common sequence of structural and metamorphic transformations of the Armovka rocks is as follows: Fracturing and recrystallization, low-temperature alteration (such as chloritization), acid leaching processes (muscovitization and superimposed quartz veins). Local albitization is characteristic of metabasites and occurs before deformation and low-temperature alteration. Albite, amphibole, white mica, and chlorite are typical retrograde minerals in the rock matrix of the Armovka Formation.

The processes of albitization lead to the formation of large poikiloblastic plagioclases (albite) of metamorphic origin up to 3 mm in size. They have a particular “cribriform” shape and contain inclusions of matrix minerals such as epidote, amphibole, and muscovite (Figure 8b). These mineral inclusions were captured during overgrowth of the albite poikiloblasts. Sometimes plagioclases are saussuritized along grain boundaries.

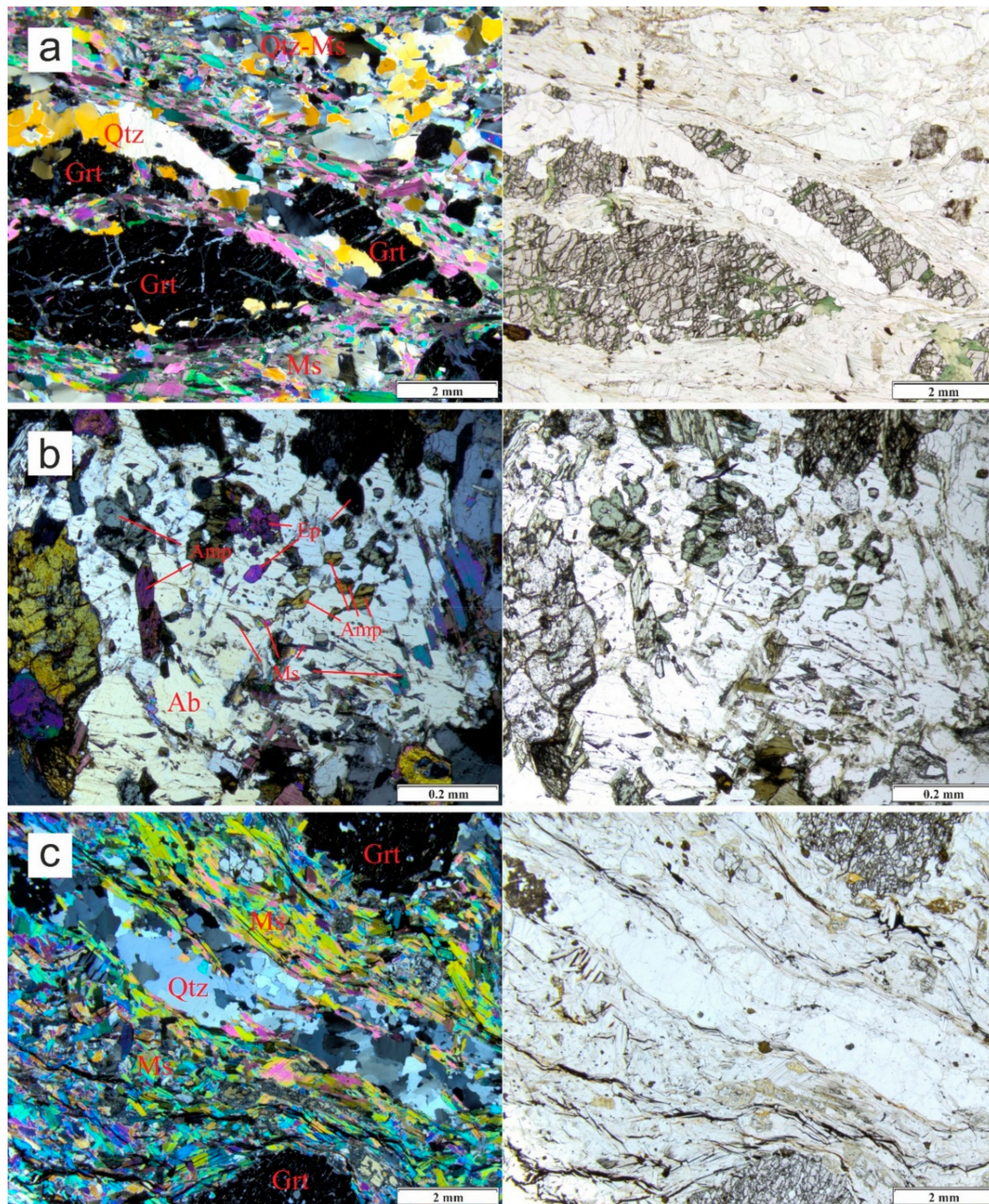


Figure 8. Photomicrographs of the Armovka Formation rocks in transmitted, cross-polarized light (left), and in plane-polarized light (right). (a) Brittle deformation of garnet porphyroblast replaced by chlorite in cracks, orientated muscovite aggregates caused by its ductile deformation, and quartz lenses and veins. (b) Large “cribriform” poikiloblastic plagioclase (albite) grain with inclusions of matrix minerals. (c) Abundant muscovitization and superimposed quartz veins. Ab—albite; Amp—amphibole; Ep—epidote; Grt—garnet; Ms—muscovite; Qtz—quartz.

During fracturing and recrystallization mechanically strong garnet grains were subjected to brittle deformation and broken down, while mica underwent ductile deformation surrounding strong grains

of other minerals (Figure 8a). Most rocks were influenced by shear deformations characteristic of Armovka nappe. During the low-grade stage some of the silicates were hydrated, i.e., garnet was replaced by chlorite, amphibole was replaced by biotite and then chlorite; biotite is frequently replaced by muscovite with the release of magnetite. Chlorites frequently occur along cracks crosscutting the garnets and replace the amphiboles and biotites forming grains with sagenitic rutile in the last case. Chlorites in the studied rocks have low-Fe and medium-Al compositions of clinocllore (pynochlorite) and penninite.

Acid leaching processes are widespread and resulted in the formation of quartz veins and abundant muscovite zones (Figure 8c). Quartz lenses and veins have thickness of up to several millimeters. Their formation is the latest process because they are not subjected to tectonic deformation unlike the main matrix minerals of the rocks and do not have any planar structure.

5. Conclusions

The petrological and electron microprobe study of sulfide-bearing gneisses and amphibolites of the Armovka Formation (Fore Range zone of the Greater Caucasus) show that pyrite and chalcopyrite can be considered as a new type of mineral container capable of preserving information about the initial mineral composition of rocks and their metamorphic evolution. Sulfides of the metamorphic rocks of the Armovka Formation contain inclusions of high-pressure minerals such as omphacite, phengite, garnet, and paragonite.

Phengite barometry yields pressures from 1.7 ± 0.2 to 1.9 ± 0.2 GPa for a temperature of 600 ± 40 °C. This estimation is almost identical to the P – T calculations for eclogites bodies embedded in the Armovka rocks—a minimum pressure of 1.6 ± 0.2 GPa and a temperature of 680 ± 40 °C [23]. It allows us to assume that the studied metamorphic rocks of the Armovka Formation were immersed in a subduction zone reaching conditions of eclogite facies metamorphism, formed a coherent subduction complex together with eclogites, and then were together exhumed to the surface.

The studied high-pressure rocks were affected by the pervasive low-grade metamorphism. The common sequence of structural and metamorphic evolution of the Armovka rocks was as follows: (1) Fracturing and recrystallization; (2) low-temperature alteration (such as chloritization); (3) acid leaching processes (muscovitization and superimposed quartz veins). Some metabasic rocks were subjected to albitization in their early stages of structural evolution. Significant alteration has removed the information about initial peak pressure conditions, which only were preserved in mineral inclusions within sulfides, as described here, and possibly in garnet although this is out of the scope of the present study.

Author Contributions: Field work, V.A.K. and A.V.L.; Conceptualization, V.A.K. and A.N.K.; Methodology, A.N.K.; Software, S.D.I.; Analysis, A.N.K. and A.I.S.; Investigation, V.A.K. and A.N.K.; Writing, Review and Editing, V.A.K., E.P.K., and A.V.L.; Visualization, E.P.K.

Funding: The work was conducted under a state contract № 0144-2014-0089 (IPE RAS).

Acknowledgments: The authors thank K.V. Van (IEM RAS) for his assistance in conducting microprobe studies. The authors would also like to thank the two anonymous reviewers for their valuable comments and suggestions to improve the manuscript and for the revision of the English text.

Conflicts of Interest: Authors declare no conflict of interest.

References

1. England, P.C.; Thompson, A.B. Pressure–temperature–time paths of regional metamorphism I. Heat transfer during the evolution of regions of thickened continental crust. *J. Petrol.* **1984**, *25*, 894–928. [[CrossRef](#)]
2. Chopin, C.; Ferraris, G. Mineral Chemistry and Mineral Reactions in UHPM Rocks. In *EMU Notes in Mineralogy*; EMU: Jena, Germany, 2003; pp. 191–227.
3. Godard, G. Eclogites and their geodynamic interpretation: A history. *J. Geodyn.* **2001**, *32*, 165–203. [[CrossRef](#)]

4. Gerya, T.; Stöckhert, B.; Perchuk, A.L. Exhumation of high-pressure metamorphic rocks in a subduction channel: A numerical simulation. *Tectonics* **2002**, *21*, 1–19. [[CrossRef](#)]
5. Smye, A.J.; Greenwood, L.V.; Holland, T.J.B. Garnet–chloritoid–kyanite assemblages: Eclogite facies indicators of subduction constraints in orogenic belts. *J. Metamorph. Geol.* **2010**, *28*, 753–768. [[CrossRef](#)]
6. Somin, M.L. Pre-Jurassic basement of the Greater Caucasus: Brief overview. *Turk. J. Earth Sci.* **2011**, *20*, 545–610.
7. Van der Straaten, F.; Schenk, V.; John, T.; Gao, J. Blueschist-facies rehydration of eclogites (Tianshan, NW-China): Implications for fluid-rock interaction in the subduction channel. *Chem. Geol.* **2008**, *255*, 195–219. [[CrossRef](#)]
8. Li, J.L.; Klemd, R.; Gao, J.; Jiang, T.; Song, Y.H. A common high-pressure metamorphic evolution of interlayered eclogites and metasediments from the ‘ultrahigh-pressure unit’ of the Tianshan metamorphic belt in China. *Lithos* **2015**, *226*, 169–182. [[CrossRef](#)]
9. Klemd, R.; John, T.; Scherer, E.E.; Rondenay, S.; Gao, J. Changes in dip of subducted slabs at depth: petrological and geochronological evidence from HP-UHP rocks (Tianshan, NW-China). *Earth Planet. Sci. Lett.* **2011**, *310*, 9–20. [[CrossRef](#)]
10. Klemd, R.; Gao, J.; Li, J.L.; Meyer, M. Metamorphic evolution of (ultra)-high-pressure subduction-related transient crust in the South Tianshan Orogen (Central Asian Orogenic Belt): Geodynamic implications. *Gondwana Res.* **2015**, *28*, 1–25. [[CrossRef](#)]
11. Gamkrelidze, I.; Shengelia, D.M. Precambrian–Paleozoic Regional Metamorphism. In *Granitoid Magmatism and Geodynamics of the Caucasus*; Scientific World: Moscow, Russia, 2005; p. 460.
12. Adamia, S.; Zakariadze, G.; Chkhotua, T.; Sadradze, N.; Tsereteli, N.; Chabukiani, A.; Gventsadze, A. Geology of the Caucasus: A Review. *Turk. J. Earth Sci.* **2011**, *20*, 489–544.
13. Kamzolkin, V.A.; Latyshev, A.V.; Vidyapin, Y.P.; Somin, M.L.; Smul’skaya, A.I.; Ivanov, S.D. Late Vendian complexes in the structure of metamorphic basement of the Fore Range zone, Greater Caucasus. *Geotectonics* **2018**, *52*, 331–345. [[CrossRef](#)]
14. Kulakova, E.P.; Kamzolkin, V.A.; Latyshev, A.V.; Vidjapin, Y.u.P.; Somin, M.L.; Ivanov, S.D. New data on the structure and age of the crystalline basement of the Fore Range of the Greater Caucasus. In Proceedings of the Geophysical Research Abstract, EGU General Assembly 2019, Vienna, Austria, 7–12 April 2019.
15. Leonov, Y.G. *Greater Caucasus in the Alpine Epoch*; GEOS: Moscow, Russia, 2007; p. 368.
16. Lavrishev, V.A.; Prutskiy, N.I.; Semenov, V.M. *State Geological Map of the Russian Federation, Scale 1:200 000, Sheet K-37-V (Krasnaya Poliana), Explanatory Note*; VSEGEI: St.-Petersburg, Russia, 2000.
17. Somin, M.L. Geological Characteristics of the Fore Range and Main Range Zones, Great Caucasus. In *Petrology of Metamorphic Complexes of the Great Caucasus*; Nauka press: Moscow, Russia, 1991; pp. 18–45.
18. Afanas’ev, G.D.; Ploshko, V.V.; Shport, N.P. Eclogite of the Fore Range Zone of the Greater Caucasus. *Izv. Akad. Nauk SSSR* **1969**, *187*, 1379–1382.
19. Tatrishvili, N.F. About a finding of eclogites in the Greater Caucasus. *Izv. Akad. Nauk SSSR* **1970**, *190*, 944–946.
20. Ploshko, V.V.; Shport, N.P.; Knyazeva, D.N. New findings of eclogites in the Caucasus. *Izv. Akad. Nauk SSSR* **1977**, *236*, 1196–1198.
21. Ploshko, V.V.; Shport, H.G. Eclogite formation in the Great Caucasus. *Izv. Akad. Nauk SSSR* **1974**, *12*, 60–71.
22. Perchuk, A.L. Metamorphism of the kyanite eclogite of the Red Cliff locality, Fore Range of the Greater Caucasus. *Petrology* **1993**, *1*, 98–109.
23. Perchuk, A.L.; Philippot, P. Rapid cooling and exhumation of eclogitic rocks from the Great Caucasus, Russia. *J. Metamorph. Geol.* **1997**, *15*, 299–310. [[CrossRef](#)]
24. Perchuk, A.L. Petrology and Mineral Chronometry of the Crust Eclogites. Ph.D. Thesis, IGEM RAS, Moscow, Russia, 2003.
25. Whitney, D.L.; Evans, B.W. Abbreviations for names of rock-forming minerals. *Am. Mineral.* **2010**, *95*, 185–187. [[CrossRef](#)]
26. Li, J.L.; Gao, J.; Klemd, R.; John, T.; Wang, X.S. Redox processes in subducting oceanic crust recorded by sulfide-bearing high-pressure rocks and veins (SW Tianshan, China). *Contrib. Mineral. Petrol.* **2016**, *171*, 72–95. [[CrossRef](#)]
27. Morimoto, N.; Fabries, J.; Ferguson, A.K.; Ginzburg, I.V.; Ross, M.; Seifert, F.A.; Zussman, J.; Aoki, K.; Gottardi, G. Nomenclature of pyroxenes. *Am. Mineral.* **1988**, *73*, 1123–1133.

28. Simpson, G.D.H.; Thompson, A.B.; Connolly, J.A.D. Phase relations, singularities and thermobarometry of metamorphic assemblages containing phengite, chlorite, biotite, K-feldspar, quartz and H₂O. *Contrib. Mineral. Petrol.* **2000**, *139*, 555–569. [[CrossRef](#)]
29. Drits, V.A.; Kossovskaya, A.G. *Clay Minerals: Mica, Chlorites*; Nauka press: Moscow, Russia, 1991; p. 176.
30. Kamzolkin, V.A.; Ivanov, S.D.; Konilov, A.N. Empirical phengite geobarometer: background, calibration, and application. *Geol. Ore Depos.* **2016**, *58*, 613–622. [[CrossRef](#)]



© 2019 by the authors. Licensee MDPI, Basel, Switzerland. This article is an open access article distributed under the terms and conditions of the Creative Commons Attribution (CC BY) license (<http://creativecommons.org/licenses/by/4.0/>).